Article

Structural Features That Stabilize ZnO Clusters: An Electronic Structure Approach

Csaba E. Szakacs [1,†]**, Erika F. Merschrod S.** [1,*] **and Kristin M. Poduska** [1,2,*]

[1] Department of Chemistry, Memorial University, St. John's NL A1B3X7, Canada;
  E-Mail: cszakacs@mun.ca
[2] Department of Physics and Physical Oceanography, Memorial University,
  St. John's NL A1B3X7, Canada

[†] Current address: Énergie Matériaux Télécommunications, Institut National de la Recherche
  Scientifique (INRS), 1650 boulevard Lionel-Boulet, Varennes QC J3X1P7, Canada.

[*] Authors to whom correspondence should be addressed; E-Mails: erika@mun.ca (E.F.M.S.);
  kris@mun.ca (K.M.P.); Tel.: +1-709-864-8765 (E.F.M.S.); +1-709-864-8890 (K.M.P.);
  Fax: +1-709-864-3702 (E.F.M.S.); +1-709-864-8739 (K.M.P.).

Abstract: We show that a simple approach to building small computationally inexpensive clusters offers insights on specific structural motifs that stabilize the electronic structure of ZnO. All-electron calculations on Zn_iO_i needle ($i = 6$, 9, 12, 15, and 18) and plate ($i = 9$ and 18) clusters within the density functional theory (DFT) formalism show a higher stability for ZnO needles that increases with length. Puckering of the rings to achieve a more wurtzite-like structure destabilizes the needles, although this destabilization is reduced by going to infinite needles (calculated using periodic boundary conditions). Calculations of density of states (DOS) curves and band gaps for finite clusters and infinite needles highlight opportunities for band-gap tuning through kinetic control of nanocrystal growth.

Keywords: ZnO; electronic structure; band structure; DFT calculations; ZnO clusters

1. Introduction

Zinc oxide (ZnO), a wide-gap semiconductor, has emerged as a prominent material with potential optoelectronics uses [1]. Because many applications involve polycrystalline or nanostructured ZnO, understanding the electronic structure differences among bulk, films, microscale, and nanoscale particles is critical [2–4]. A promising way to address this challenge is to use theoretical methods to study model clusters, particularly in probing structures that lie between molecular and bulk [5,6].

One approach to creating structural models of clusters is to maintain stoichiometry, preserve neutrality and limit the number of dangling bonds [7]. This approach is validated with recent theoretical studies on very small clusters showing that charge and excess oxygen lead to instability [8]. However, this still allows for many possible geometries, and it is challenging to find a true global minimum energy structure. Numerous theoretical studies of stoichiometric, neutral Zn_iO_i type clusters have explored optimized geometries for a range of cluster sizes, and some discuss energy changes related to the specific structural features [9–13]. A prevalent theoretical observation is that a cage-like structural motif shows increased stability for smaller-sized clusters, while a wurtzite-like structure shows increased stability for larger clusters. However, the scant experimental evidence for cage-like clusters is limited to small structures in the gas phase, which makes the size at which the transition to a bulk-like (wurtzite) structure occurs an important issue of debate [10,14]. Unfortunately, this is an expensive proposition to explore from a computational perspective, since geometry optimization of large clusters can be time prohibitive.

To address this challenge, we seek to identify structural features linked to electronic stability for clusters of intermediate size, thereby providing the basis for a more general understanding of the transition from cluster to bulk-like features. Our geometries are based on clusters excised from a wurtzite structure, an approach that has proved successful for understanding ZnS structures [15]. Our approach for finding stabilizing structural motifs offers an interesting alternative to other options for predicting crystal shape (such as surface energy calculations). It also demonstrates the value of model design based on an understanding of electronic structure, rather than relying solely on computationally intensive searches for energy minima in a broader potential energy landscape.

2. Computational Methods

Geometry optimization, vibrational analysis, and molecular orbital calculations for Zn_iO_i clusters (with i ranging from 6 to 18) were carried out using density functional theory (DFT). Optimizations for these finite geometries utilized the hybrid B3LYP functional [16,17] with the medium-sized 6–31G(d) basis set. Vibrational analyses indicated that these are true local minima. The B3LYP functional yielded reasonable results for small ZnO clusters in earlier studies [18] and has been reliable for predicting band gap values for a variety of metal oxides [19].

The extended systems were modeled within the DFT formalism as well, under periodic boundary conditions (PBC). Geometry optimization of the infinite needles was performed using the PBE [20] functional and the 6–31G(d) basis set. Convergence in total energy and band gap for calculations with varying numbers of k points indicates that 8 k points provides reliable results on an efficient time scale.

For comparison between finite clusters and infinite needles, energies for the $Zn_{18}O_{18}$ clusters were recalculated with the PBE functional. As expected, total energies and band gap energies are significantly

different from calculations using different functionals, but the trends for finite systems between B3LYP and PBE calculations remained the same. We do not anticipate qualitatively different behaviour for the shorter needles; our main concern is to establish that changing the functional does not qualitatively change the apparent electronic structure of the needle.

Scaled energies are used throughout to allow a direct comparison between energies of clusters with different sizes. Total energies will necessarily scale with the cluster size, regardless of stability. Thus, the scaled energy $E_S = E/N$, where E is the total energy and N is the number of atoms in the cluster or unit cell, is corrected for cluster size. We also present scaled relative energies E_{SR}, which are calculated relative to the lowest energy conformer in the set. Energies calculated with different theory, functionals or basis sets cannot be directly compared. For example, changing basis set would also yield different results for energy and band gap, although not as dramatic as the change in functional. Our emphasis is on trends, not absolute energies.

All theoretical methods employed during the simulations were used as implemented in the Gaussian software package [21,22]. Molecular structures were visualized with GaussView 5.0.8 (Gaussian Inc.), while JMol [23] was used to visualize molecular orbital isosurfaces. In order to obtain density of states (DOS) curves, crystal orbital overlap population (COOP) diagrams, and carry out charge decomposition analysis (CDA), the output was parsed and analyzed using the Qmforge [24] and GaussSum [25] programs. In this work, band gaps for finite systems are defined as the difference between the calculated energies for the lowest unoccupied molecular orbital (LUMO) and highest occupied molecular orbital (HOMO).

3. Results and Discussion

3.1. Relative Crystal Shape Stabilities

Clusters with different sizes and geometries were constructed to resemble plate- or needle-like shapes using small, chemically reasonable units to build larger clusters. This approach saves considerable calculation time while still allowing us to probe which structural features play the most important role in stabilizing the overall structure. The final optimized geometries are depicted in Figure 1. The variation in energy based on scaled relative energy (E_{SR}) values (Figure 2a) for these clusters shows that the needle-type conformations are significantly more stable than their respective plate-like isomers. This is consistent with experimental findings for much larger ZnO nanoparticles, where needle shapes are prevalent and plate shapes typically require the use of surfactants, surface capping agents, or seeded substrate growth [1,26–32]. We selected these models to highlight the issues with lateral versus longitudinal growth. In studying needle growth, the Zn_3O_3 unit provided the most systematic building block, rather than adding individual atoms or pairs of Zn/O atoms.

Molecular orbital calculations show that needle stabilization with respect to plates, and the further stabilization with longer needles, comes from the transformation of lone pairs into bonds. When bringing rings together to form needles, the principal orbital interactions involve a set of occupied orbitals that are primarily oxygen-based (as shown in Figure 3) along with unoccupied orbitals that have increasing Zn character at higher energies. We characterize these occupied orbitals as lone-pair-like because they

are nearly non-bonding within the ring, or even Zn-O anti-bonding (Figure 3a). The "lone pair" lobes are oriented in a direction that promotes bond formation perpendicular to the ring plane, not laterally as would be required for plate-like growth.

Figure 1. Optimized geometries of needle- and plate-type Zn_iO_i clusters, where $i = 9$ and 18. Zn atoms are shown in gray, while O atoms are depicted in black.
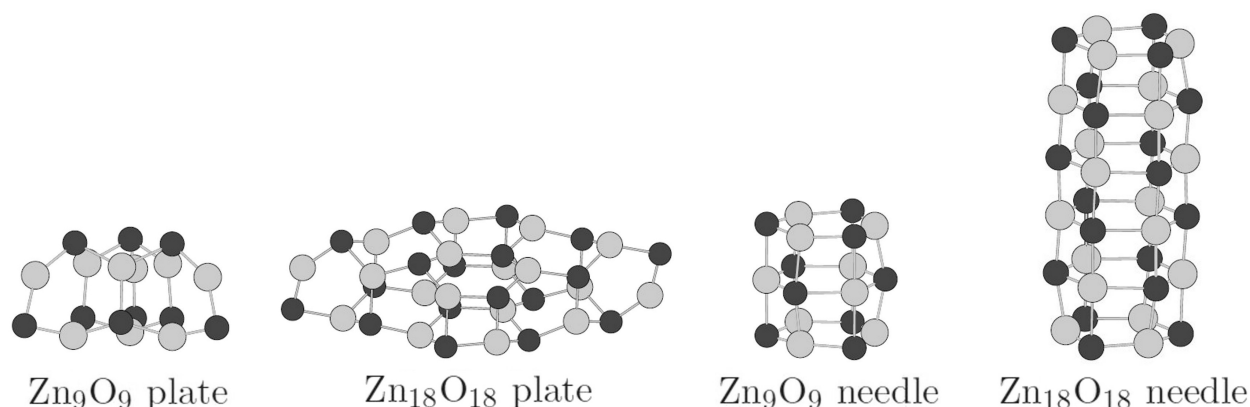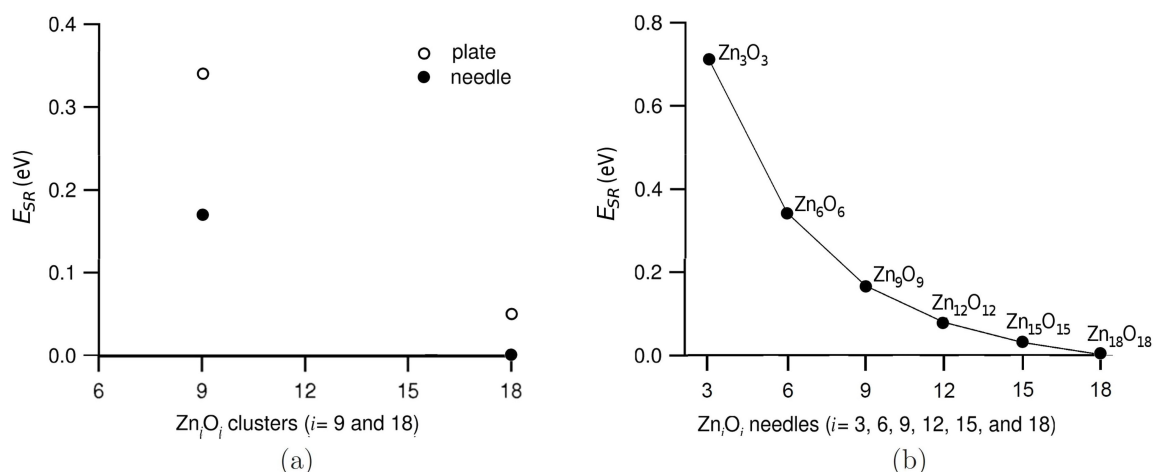

Zn_9O_9 plate $Zn_{18}O_{18}$ plate Zn_9O_9 needle $Zn_{18}O_{18}$ needle

Figure 2. Scaled relative energies (E_{SR}) of ZnO clusters, showing differences between (**a**) plate and needle clusters; and (**b**) different length Zn_iO_i needles, where $i = 3, 6, 9, 12, 15,$ and 18. (The line connecting data points in (**b**) is simply a guide to the eye.) To obtain the scaled relative energy, the energy relative to the lowest energy conformer was divided by the number of atoms in the cluster.

(a)   (b)

While the orbitals in question are not contributing much to intra-ring Zn-O bonding (Figure 3a, the HOMO for Zn_3O_3), some do present more Zn-O intra-ring bonding (Figure 3b, the HOMO-3). As a result, the formation of inter-ring bonds comes at the cost of some intra-ring bonding. The shift in inter- and intra-ring bonding is quantified by overlap population (Table 1), where a higher overlap population value indicates a stronger bond (all else being equal). The weakening of intra-ring bonding (Zn-O overlap population drops from 0.236 upon adding rings) is more than offset by the new bonds formed non-zero Zn-O overlap population between rings, leading to the overall stabilization (Figure 2b).

Figure 3. Molecular orbital isosurfaces for two representative lone-pair-like orbitals in a Zn_3O_3 ring. Phases are indicated with light and dark shading, and 0.02 is the isovalue. (**a**), the HOMO, is slightly Zn-O anti-bonding while (**b**), the HOMO-3, shows some Zn-O bonding, as indicated by overlap population values.
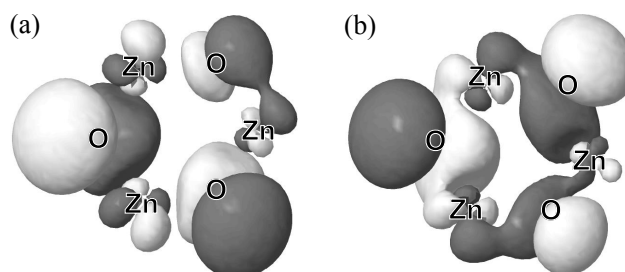

Table 1. Average overlap population values for Zn-O bonds within rings (OP_{wr}) and between rings (OP_{br}) of needles of various lengths. A higher overlap population value indicates a stronger bond. Zn-O overlap population within the ring drops upon growing the needle from a single Zn_3O_3 ring, but the needle growth results in a positive overlap population between Zn and O on adjacent rings.

Needles	OP_{wr}		OP_{br}
	Terminal rings	**Middle rings**	
Zn_3O_3	0.236	-	-
Zn_6O_6	0.167	-	0.170
Zn_9O_9	0.192	0.077	0.156
$Zn_{18}O_{18}$	0.188	0.110	0.152

3.2. Toward Wurtzite: Puckering and Extending the Needles

While the needles shown in Figure 1 do share some similarities with the wurtzite structure that is characteristic of most nanostructured ZnO, there are two major differences. First, the Zn-O rings are nearly flat while those in wurtzite would be strongly puckered to yield tetrahedral coordination environments for both the O and the Zn. Second, given the small size of our model clusters relative to many experimentally-achieved nanostructures, it is possible that their electronic structure is artificially dominated by terminating atoms.

To explore the impact of these differences on the electronic structures and stability trends, we created extended puckered and unpuckered needles by modeling them on finite clusters (shown in Figure 4) and using periodic boundary conditions with a Zn_6O_6 repeat unit. This yields one-dimensional extended molecules that we denote as $^1_\infty[Zn_6O_6]$. Our comparisons between finite and infinite system energies are based on calculations with the PBE functional [20] required for the calculations. The puckering perturbation has essentially no effect on energy for the infinite needles, which suggests that longer finite needles may be attainable in either geometry or perhaps with an intermediate degree of puckering.

However, puckering is a destabilizing interaction for the finite needles we calculated, as shown in the relative scaled energies in Table 2.

Figure 4. (**a**) Unpuckered *vs.* (**b**) puckered needles. These structures are also the unit cells used for infinite needle calculations.
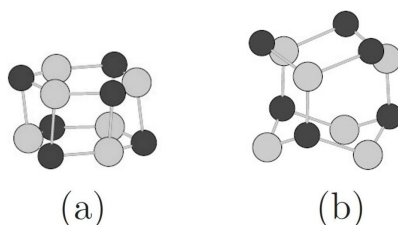

(a)   (b)

Table 2. Scaled energies (E_S) and relative energies (E_{SR}), in eV, between unpuckered and puckered needles, calculated with the PBE functional. For the lowest energy conformation, a relative energy of zero is assigned.

Needles	E_S	E_{SR}
unpuckered $Zn_{18}O_{18}$	–25224.683	0
puckered $Zn_{18}O_{18}$	–25224.178	0.505
unpuckered $^1_\infty[Zn_6O_6]$	–25224.732	0
puckered $^1_\infty[Zn_6O_6]$	–25224.727	0.004

A bonding analysis illustrates how destabilization arises from puckering. In the DOS plot for the finite needle (Figure 5a), there is a shift of states toward the gap region upon puckering (Figure 5b). These states are primarily O-based, as seen in the projected DOS curves for oxygen (Figure 5a and b, shaded regions). The COOP curves in Figure 5c for intra-ring Zn-O bonds indicate that the energy shifts coincide with shifts in bonding character: states that are bonding (positive) in the unpuckered needle become non-bonding (zero) or antibonding (negative) in the puckered needle. In other words, the destabilization comes from further reduced bonding at already undercoordinated atoms [15,33]. The destabilization from puckering disappears for infinite needles, and it would likewise disappear for infinite clusters (*i.e.*, bulk ZnO) where all atoms are fully coordinated.

Interestingly, although the energies of the puckered and unpuckered infinite needles are very similar, they show a rather different band structure: the unpuckered needle shows an indirect band gap, while puckering results in a larger, direct band gap (band diagrams not shown). Experimentally, wurtzite-type ZnO, which is most similar to our unpuckered system, also has a direct band gap [1]. In our calculations, different band gap energies appear for $Zn_{18}O_{18}$ puckered and unpuckered finite needles, though to a lesser extent (see Table 3). Note that these band gap values for finite clusters are calculated with the PBE functional, which is known to yield unrealistically low values compared with experimental observations [34,35]. Nevertheless, the trend in band gap changes is meaningful. We also note that the band structure of similar unpuckered and puckered needles have been calculated recently by others using

different functionals, and while their band gap energies also vary greatly with functional, the trends are consistent with what we observe here [36].

Figure 5. Density-of-states (DOS) curves for finite unpuckered (**a**) and puckered (**b**) $Zn_{18}O_{18}$ needles. The shaded regions indicate O-based states. (**c**) COOP curves showing intra-ring Zn-O overlap population in the unpuckered (solid line) and puckered (dashed line) needles.
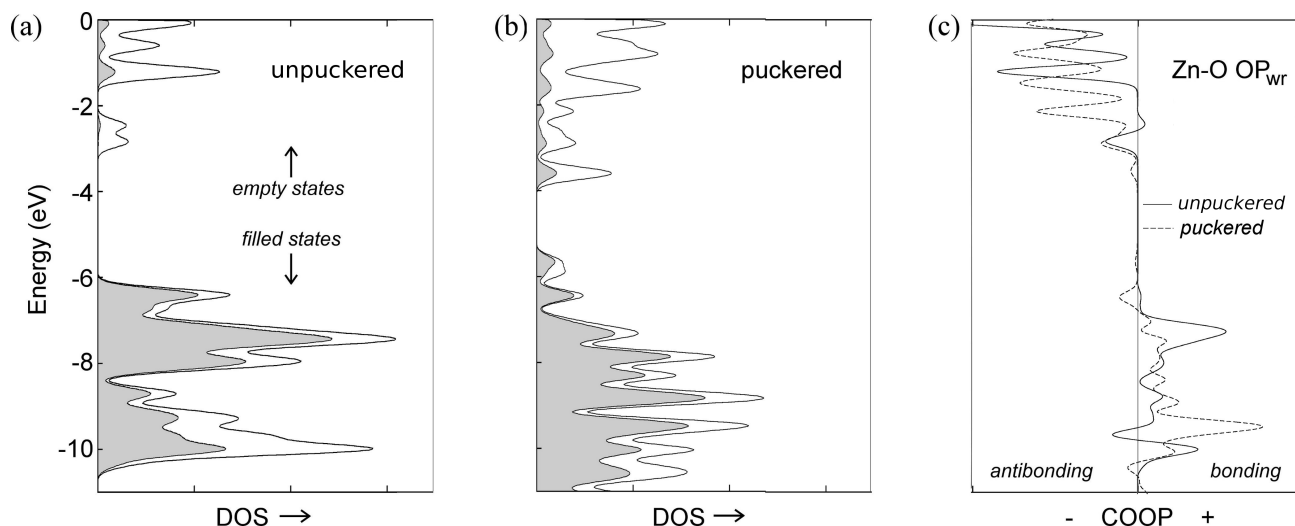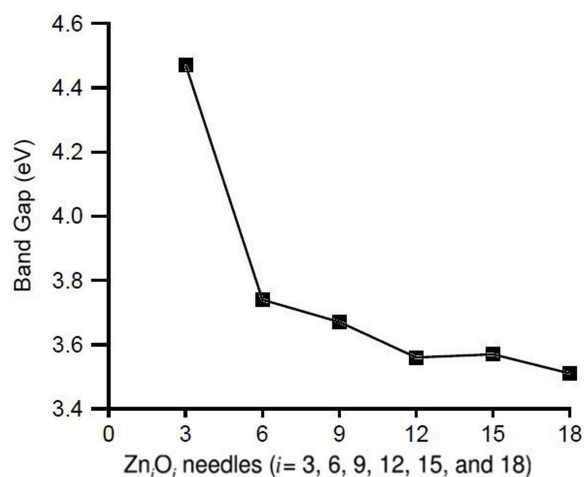

Table 3. Band gaps for finite and infinite needles that are based on either unpuckered or puckered building blocks. The infinite unpuckered needle shows an indirect band gap, while the infinite puckered needle shows a direct gap.

Needles	Band Gap (eV)
unpuckered $Zn_{18}O_{18}$	1.70
puckered $Zn_{18}O_{18}$	1.67
unpuckered $^1_\infty[Zn_6O_6]$	1.60
puckered $^1_\infty[Zn_6O_6]$	1.84

Calculations on finite systems, where the B3LYP functional could be employed, yield band gap values that are more comparable to experimental values for bulk ZnO ($\sim$3.3 eV) [1]. While we are not concerned with replicating absolute band gap energies, it is useful to note where the calculations fall close to experimental values. Figure 6 shows the variation of band gap values for finite unpuckered needles as a function of needle growth. We note that plates show smaller band gaps (3.18 eV for $i = 9$ and 3.36 eV for $i = 18$) due to low-lying Zn-based acceptor states that are based primarily on atoms in the core of the plate and can be related to the molecular orbitals involved in needle growth. In other words, the stabilization achieved by adding atoms to the end of the needle removes the low-lying acceptor states from the gap region, thus widening the band gap.

Figure 6. Band gap trend for unpuckered Zn_iO_i needles, i = 3, 6, 9, 12, 15, and 18, based on the B3LYP functional.

4. Conclusions

Our electronic structure calculations enhance understanding of the relative thermodynamic stabilities of two prominent ZnO nanocrystal shapes: plates and needles. In our clusters, an overall stability of needles is observed, and this stabilization increases with the number of stacked rings, suggesting favored growth of the needle-type ZnO. The structural element at the root of this stabilization is the formation of ...O–Zn–O... chains perpendicular to the rings.

Despite the artificially small size of our calculated clusters, we show that the crystal shape trends they imply are consistent with experimental observations for ZnO particles [1–4]. The agreement between energy stability trends from cluster calculations and preferred shapes in real-life ZnO nanostructures offers tremendous possibilities for using experimentally inspired computational models to both understand and predict crystal shape based on electronic structure arguments. The prevalence of the cage-like motifs as lowest energy structures in many earlier theoretical studies—for which there is little experimental backing—would suggest that larger cluster sizes would be required in order to obtain experimentally-relevant electronic structure information. The success of our approach shows that bigger clusters are not necessarily the only way to bridge this gap between computationally-practical models and experimental measurements.

We acknowledge that there are many other factors that can influence band gap values, including surface functionalization [37] or termination [38] and doping [39] effects inherent to many experimental preparation procedures, but we do not consider those here. What our results do hint at, though, is the possibility of band gap tuning with changes in crystal shape. Structures that are calculated to be less stable in a thermodynamic sense may nonetheless be kinetically stable, and therefore experimentally attainable. Therefore, our exploration of different types of ZnO clusters can serve as a guide for the design of structure and electronic properties in nanoparticles of this multi-purpose material.

Acknowledgements

References

1. Özgür, U.; Alivov, Y.I.; Liu, C.; Teke, A.; Reshchikov, M.A.; Doğan, S.; Avrutin, V.; Cho, S.J.; Morkoç, H. A comprehensive review of ZnO materials and devices. *J. Appl. Phys.* **2005**, *98*, 041301–041404.

2. Brewster, M.M.; Zhou, X.; Lu, M.Y.; Gradečak, S. The interplay of structural and optical properties in individual ZnO nanostructures. *Nanoscale* **2012**, *4*, 1455–1462.

3. Cui, J. Zinc oxide nanowires. *Mater. Charact.* **2012**, *64*, 43–52.

4. Spencer, M.J. Gas sensing applications of 1D-nanostructured zinc oxide: Insights from density functional theory calculations. *Prog. Mater. Sci.* **2012**, *57*, 437–486.

5. Mowbray, D.J.; Martínez, J.I.; Calle-Vallejo, F.; Rossmeisl, J.; Thygesen, K.S.; Jacobsen, K.W.; Nørskov, J.K. Trends in metal oxide stability for nanorods, nanotubes, and surfaces. *J. Phys. Chem. C* **2011**, *115*, 2244–2252.

6. Oliva, J.M.; Llunll, M.; Alemany, P.; Canadell, E. Quantitative *vs.* qualitative approaches to the electronic structure of solids. *J. Solid State Chem.* **2003**, *176*, 375–389.

7. Lü, X.; Xu, X.; Wang, N.; Zhang, Q.; Ehara, M.; Nakatsuji, H. Cluster modeling of metal oxides: How to cut out a cluster? *Chem. Phys. Lett.* **1998**, *291*, 445–452.

8. Gunaratne, K.D.D.; Berkdemir, C.; Harmon, C.L.; Castleman, A.W., Jr. Investigating the relative stabilities and electronic properties of small zinc oxide clusters. *J. Phys. Chem. A* **2012**, *116*, 12429–12437.

9. Caddeo, C.; Malloci, G.; de Angelis, F.; Colombo, L.; Mattoni, A. Optoelectronic properties of $(ZnO)_{60}$ isomers. *Phys. Chem. Chem. Phys.* **2012**, *14*, 14293–14298.

10. Malloci, G.; Chiodo, L.; Rubio, A.; Mattoni, A. Structural and optoelectronic properties of unsaturated ZnO and ZnS nanoclusters. *J. Phys. Chem. C* **2012**, *116*, 8741–8746.

11. Zhang, S.; Zhang, Y.; Huang, S.; Liu, H.; Wang, P.; Tian, H. Theoretical investigation of growth, stability, and electronic properties of beaded ZnO nanoclusters. *J. Mater. Chem.* **2011**, *21*, 16905–16910.

12. Wang, X.; Wang, B.; Tang, L.; Sai, L.; Zhao, J. What is atomic structures of $(ZnO)_{34}$ magic cluster. *Phys. Lett. A* **2010**, *374*, 850–853.

13. Sanyal, B.; Mookerjee, A. Study of the electronic and structural properties of ZnO clusters. *Int. J. Mod. Phys. B* **2010**, *24*, 3297–3309.

14. Zhao, M.; Xia, Y.; Tan, Z.; Liu, X.; Mei, L. Design and energetic characterization of ZnO clusters from first-principles calculations. *Phys. Lett. A* **2007**, *372*, 39–43.

15. Azpiroz, J.M.; Mosconi, E.; de Angelis, F. Modeling ZnS and ZnO nanostructures: Structural, electronic, and optical properties. *J. Phys. Chem. C* **2011**, *115*, 25219–25226.

16. Becke, A.D. Density-functional thermochemistry. III. The role of exact exchange. *J. Chem. Phys.* **1993**, *98*, 5648–5652.

17. Lee, C.; Yang, W.; Parr, R.G. Development of the Colle-Slavetti correlation-energy formula into a functional of the electron density. *Phys. Rev. B* **1988**, *37*, 785–789.

18. Matxain, J.M.; Fowler, J.E.; Ugalde, J.M. Small clusters of II-VI materials: Zn_iO_i, i = 1 − 9. *Phys. Rev. A* **2000**, *62*, 053201–053211.

19. Muscat, J.; Wander, A.; Harrison, N.M. On the prediction of band gaps from hybrid functional theory. *Chem. Phys. Lett.* **2001**, *342*, 397–401.

20. Perdew, J.P.; Burke, K.; Ernzerhof, M. Generalized gradient approximation made simple. *Phys. Rev. Lett* **1996**, *77*, 3865–3868.

21. Frisch, M.J.; Trucks, G.W.; Schlegel, H.B.; Scuseria, G.E.; Robb, M.A.; Cheeseman, J.R.; Montgomery, J.A.J.; Vreven, T.; Kudin, K.N.; Burant, J.C.; *et al. Gaussian 03, Revision D.01*; Gaussian, Inc.: Wallingford, CT, USA, 2004.

22. Frisch, M.J.; Trucks, G.W.; Schlegel, H.B.; Scuseria, G.E.; Robb, M.A.; Cheeseman, J.R.; Scalmani, G.; Barone, V.; Mennucci, B.; Petersson, G.A.; *et al. Gaussian 09, Revision A.1*; Gaussian Inc.: Wallingford, CT, USA, 2009.

23. Jmol: An open-source Java viewer for chemical structures in 3D. Available online: http://www.jmol.org/ (accessed on 29 May 2013).

24. Tenderholt, A.L. QMForge, Version 2.1. Available online: http://qmforge.sourceforge.net (accessed on 29 May 2013).

25. O'Boyle, N.M.; Tenderholt, A.L.; Lagner, K.M. cclib: A library for package-independent computational chemistry algorithms. *J. Comput. Chem.* **2008**, *29*, 839–845.

26. Illy, B.; Shollock, B.A.; MacManus-Driscoll, J.L.; Ryan, M.P. Electrochemical growth of ZnO nanoplates. *Nanotechnology* **2005**, *16*, 320–324.

27. Kumar, P.S.; Raj, A.D.; Mangalaraj, D.; Nataraj, D.; Ponpandian, N.; Li, L.; Chabrol, G. Growth of hierarchical based ZnO micro/nanostructured films and their tunable wettability behavior. *Appl. Surf. Sci.* **2011**, *257*, 6678–6686.

28. Wang, W.; Wang, L.; Liu, L.; He, C.; Tan, J.; Liang, Y. Morphology-controlled synthesis and growth mechanism of ZnO nanostructures via the NaCl nonaqueous ionic liquid route. *CrystEngComm* **2012**, *14*, 4997–5004.

29. Gao, S.Y.; Li, H.D.; Yuan, J.J.; Yang, X.X.; Liu, J.W. ZnO nanorods/plates on Si substrate grown by low-temperature hydrothermal reaction. *Appl. Surf. Sci.* **2010**, *256*, 2781–2785.

30. Wang, J.S.; Yang, C.S.; Chen, P.I.; Su, C.F.; Chen, W.J.; Chiu, K.C.; Chou, W.C. Catalyst-free highly vertically aligned ZnO nanoneedle arrays grown by plasma assisted molecular beam epitaxy. *Appl. Phys. A* **2009**, *97*, 553–557.

31. Ahn, M.W.; Park, K.S.; Heo, J.H.; Kim, D.W.; Choi, K.J.; Park, J.G. On-chip fabrication of ZnO-nanowire gas sensor with high gas sensitivity. *Sens. Actuators B* **2009**, *138*, 168–173.

32. Xu, J.; Zhang, Y.; Chen, Y.; Xiang, Q.; Pan, Q.; Shi, L. Uniform ZnO nanorods can be used to improve the response of ZnO gas sensor. *Mater. Sci. Eng. B* **2008**, *150*, 55–60.

33. Azpiroz, J.M.; Infante, I.; Lopez, X.; Ugalde, J.M.; de Angelis, F. A first-principles study of II-VI (II = Zn; VI = O, S, Se, Te) semiconductor nanostructures. *J. Mater. Chem.* **2012**, *22*, 21453–21465.

34. Komsa, H.P.; Broqvist, P.; Pasquarello, A. Alignment of defect levels and band edges through hybrid functionals: Effect of screening in the exchange term. *Phys. Rev. B* **2010**, *81*, 205118.

35. Zhao, Y.; Truhlar, D.G. Calculation of semiconductor band gaps with the M06-L density functional. *J. Chem. Phys.* **2009**, *130*, 074103, doi: 10.1063/1.3076922.

36. Zhang, Y.; Wen, Y.H.; Zheng, J.C.; Zhu, Z.Z. Direct to indirect band gap transition in ultrathin ZnO nanowires under uniaxial compression. *Appl. Phys. Lett.* **2009**, *94*, 113114:1–113114:3.

37. Kumar, S.; Sahare, P. Observation of band gap and surface defects of ZnO nanoparticles synthesized via hydrothermal route at different reaction temperature. *Opt. Commun.* **2012**, *285*, 5210–5216.

38. Mohanta, K.; Pal, A.J. Diode junctions between two ZnO nanoparticles: Current rectification and the role of particle size (and bandgap). *Nanotechnology* **2009**, *20*, 185203, doi: 10.1088/0957-4484/20/18/185203.

39. Sans, J.A.; Sánchez-Royo, J.F.; Segura, A.; Tobias, G.; Canadell, E. Chemical effects on the optical band-gap of heavily doped ZnO: M_{III}(M = Al,Ga,In): An investigation by means of photoelectron spectroscopy, optical measurements under pressure, and band structure calculations. *Phys. Rev. B* **2009**, *79*, 195105:1–195105:9.